



Research paper

Synthesis, structural characterization and antimicrobial activities of triorganotin(IV)azo-carboxylates derived from *ortho/para*-amino benzoic acids and β -naphthol

Paresh Debnath^a, Ankit Das^a, Keisham Surjit Singh^{a,*}, Tage Yama^b, S.Sureshkumar Singh^b, Ray J. Butcher^c, Lesław Sieron^d, Waldemar Maniukiewicz^{d,*}

^a Department of Chemistry, National Institute of Technology Agartala, Jirania, Tripura (west) 799046, India

^b Department of Forestry, North Eastern Regional Institute of Science And Technology, Nirjuli, Arunachal Pradesh 791109, India

^c Department of Chemistry, Howard University, 525 College Street, NW, Washington DC 20059, USA

^d Institute of General and Ecological Chemistry, Lodz University of Technology, 90-924 Lodz, Zeromskiego 116, Poland

ARTICLE INFO

Keywords:

Tri-organotin(IV) azo-carboxylates
NMR spectroscopy
X-ray crystal structure
Antimicrobial activity

ABSTRACT

Triorganotin (IV) complexes **1–3** were synthesized by the reaction of azo-carboxylic acid *viz.* 2/4-(2-hydroxynaphthylazo)benzoic acids with appropriate triorganotin(IV) chlorides [R = Me (compounds **1** and **2**) and Bu (compound **3**)] in presence of triethyl amine base. The complexes were characterized by elemental analysis, IR and multinuclear (¹H and ¹³C- and ¹¹⁹Sn)-NMR spectroscopy. The structures and mode of coordination around tin ions in the complexes were determined by single crystal X-ray crystallography. The complexes exhibit trigonal bipyramidal geometry around tin atoms where the base of the equatorial plane is being occupied by the three alkyl groups [Me or Bu] while the axial positions are occupied by carboxylate oxygen atoms in **2** and in case of **1** and **3**, by carboxylate and phenoxide oxygen atoms, respectively. It has been found that, the crystal structure of **1** or **3** is a cyclic dimeric, whereas **2** exhibits a polymeric structure. The ¹¹⁹Sn NMR studies show that all complexes have four-coordinate structures indicating dissociation of these complexes in solution state. The complexes were also screened for their antimicrobial activity and the compound **3** was found to exhibit effective antimicrobial activity.

1. Introduction

Organotin (IV) carboxylates have been explored by several research groups for the last few decades because of their intriguing diverse molecular structures such as monomeric, dimeric, polymeric, tetrameric, oligomeric ladder, macro-cyclic, cluster, cage, 1D and 2D molecular structures etc. [1–10]. Further, organotin(IV) carboxylates have been also studied for their potential biological activities, for instance they have been found to be effective as antitumor, antibacterial, antifungal, cytotoxic, insecticidal, anti-proliferative and anti-tuberculosis etc. [9–14]. Likewise, organotin(IV) complexes with azo-carboxylates have also been studied in great details owing to their structural diversity [15–18] and promising biological properties [15–17]. Recently, we have explored the chemistry of organotin (IV) complexes with azodicarboxylic acids derived from salicylic acid and *ortho*- and *para*-amino benzoic acids [19–20]. The biological properties such as antimicrobial and antidiabetic activities as well molecular structures for

these compounds were studied. In complex described above [17], both carboxylate group of the ligands coordinated to the adjacent tin atoms exclusively in bridging bidentate fashion giving rise to a polymeric structure with trigonal bipyramidal geometry around tin atoms. The compound showed significant antimicrobial activity. In addition, more recently our group have reported molecular structures and anti-diabetic effects of triorganotin(IV) azo-carboxylates derived from amino benzoic acids and resorcinol [21]. These compounds showed promising anti-diabetic activities even higher than the standard compound acarbose and were probably the first organotin(IV) azo carboxylates that revealed this type of activity. Thus, in our recent investigation on organotin(IV) chemistry with azo-carboxylate ligands derived from *ortho*- and *para*- amino benzoic acids, we have been exploring organotin(IV) complexes for quite some time with functionalized azo carboxylates by taking different diazo-coupling moieties *viz.* salicylic acid [19,20] and resorcinol [21]. In this work our objective is to increase the number of binding sites of the carboxylate ligands which would coordinate to the

* Corresponding authors.

E-mail addresses: keisham.chem@nita.ac.in (K.S. Singh), waldemar.maniukiewicz@p.lodz.pl (W. Maniukiewicz).

<https://doi.org/10.1016/j.ica.2019.119172>

Received 26 August 2019; Received in revised form 23 September 2019; Accepted 23 September 2019

Available online 24 September 2019

0020-1693/ © 2019 Elsevier B.V. All rights reserved.

metal atom. Therefore, as a continuous effort for our research group in the design of various novel molecular structures which would exhibit potential biological activities, we are interested in further research on the chemistry of organotin(IV) complexes with different azo-carboxylates derived from *ortho* and *para* amino-benzoic acids. Thus, in this present contribution we report a new series of triorganotin (IV) complexes [R = Me (**1** and **2**); and Bu (**3**)] with azo-carboxylates obtained from diazo coupling of amino benzoic acids and β -naphthol. The synthesized complexes were characterized by elemental analysis, IR, multinuclear (^1H , ^{13}C , ^{119}Sn) NMR spectroscopy. Structures of all compounds were determined by X-ray crystallography. In addition, we have studied anti-microbial activities of the complexes and compared them with the standard antibiotics.

2. Experimental

2.1. Materials and methods

Tri-*n*-butyltin(IV) chloride, trimethyltin(IV) chloride, *o*-amino benzoic acid, *p*-amino benzoic, and triethyl amine were obtained from MERCK by purchase and were used without further purification. Solvents were dried and purified following the standard procedures. Carbon, hydrogen and nitrogen analyses were performed on a Perkin Elmer 2400 series II instrument. UV-Visible spectra of the ligands and the complexes were recorded on UV-1800 Shimadzu spectrophotometer in DMF in the range 200–800 nm while the IR spectra were obtained from Shimadzu FT-IR-8400S spectrophotometer in the range of 4000–400 cm^{-1} using KBr discs. ^1H , ^{13}C and ^{119}Sn NMR spectra were recorded on Bruker AMX 400 spectrometer measured at 400.13, 100.62 and 149.18 MHz respectively. Me_4Si was used as reference for ^1H - and ^{13}C - chemical shifts set at 0.00 ppm while Me_4Sn set at 0.00 ppm was employed as reference for ^{119}Sn - chemical shifts.

2.2. Synthesis

2.2.1. Synthesis of 2-(2-hydroxynaphthylazo) benzoic acid (H_2L^1)

The azo-carboxylate ligand 2-(2-hydroxynaphthylazo) benzoic acid [H_2L^1] was prepared by diazo-coupling reaction of *o*-amino benzoic acid with β -naphthol following analogous reported procedure [19,22,23]. *o*-Amino benzoic acid (5 g, 36.45 mmol) was mixed with 12 mL concentrated HCl and 40 mL water; the mixture was then digested in a water bath till the solution became clear. The digested solution was then kept overnight in refrigerator and then diazotized at 0–5 °C with ice cold aqueous solution of NaNO_2 (2.51 g, in 20 mL water) for about 1 h. It was then added to the alkaline solution (10% NaOH solution, 5 g in 50 mL water) of β -naphthol (5.256 g, 36.45 mmol) at about 0–2 °C with vigorous stirring. A deep red color appeared immediately and the stirring was continued for 3 h. The reaction was kept in refrigerator for overnight again and then kept at room temperature for 2–3 h. It was then acidified with dilute acetic acid to get the red precipitate of azo ligand. The product was then filtered, washed with distilled water till the filtrate became neutral and finally the product was dried on water bath. The solid mass was then recrystallized from methanol to get desired pure red crystalline product of H_2L^1 . Yield: 7.4 g, 69.4%; m.p.: 260–262 °C. Anal. calcd. for $\text{C}_{17}\text{H}_{12}\text{N}_2\text{O}_3$: C, 69.86; H, 4.14; N, 9.58%. Found: C, 69.79; H, 4.19; N, 9.60%. UV-visible (DMF) λ_{max} (nm): 252, 316, 477. IR (KBr, cm^{-1}): 3365 $\nu(\text{OH})$, 1710 $\nu(\text{COO})_{\text{asy}}$, 1448 $\nu(\text{N}=\text{N})$, 1255 $\nu(\text{C}-\text{O})$. ^1H NMR (DMSO- d_6 , 400.13 MHz) δ_{H} : 16.11 [s, 1H, OH], 8.11 [d, 1H, H-9, $J = 8.0$ Hz], 8.04 [d, 1H, H-3', $J = 8.4$ Hz], 7.78 [d, 1H, H-6, $J = 7.6$ Hz], 7.57 [d, 1H, H-4, $J = 9.6$ Hz], 7.48 [t, 1H, H-4', $J = 7.6$ Hz], 7.38 [d, 1H, H-6' $J = 7.6$ Hz], 7.30 [t, 1H, H-8, $J = 7.6$ Hz], 7.17 [t, 1H, H-5', $J = 7.6$ Hz], 7.04 [t, 1H, H-7, $J = 7.6$ Hz], 6.38 [d, 1H, H-3 $J = 9.6$ Hz] ppm; Signal due to $-\text{COOH}$ could not be detected due to solvent exchange. ^{13}C NMR (DMSO- d_6 , 100.62 MHz) δ_{C} : 178.94 [COO], 167.43 [C-2], 143.9 [C-1'], 142.46 [C-1], 134.29 [C-4], 131.36 [C-4'], 133.17 [C-5'], 130.40 [C-3']

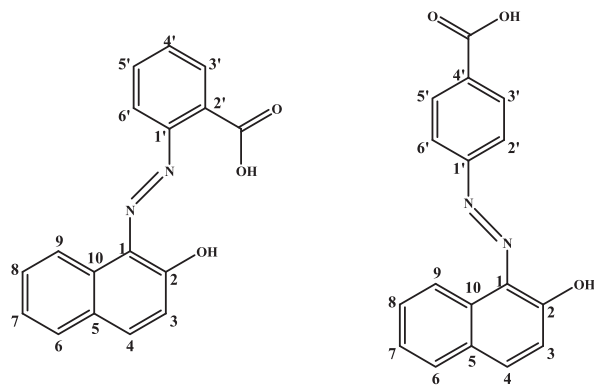
129.40 [C-10], 129.08 [C-5], 128.15 [C-6], 126.94 [C-8], 126.64 [C-9], 124.28 [C-7], 122.01 [C-6'], 116.86 [C-3], 116.12 [C-2].

2.2.2. Synthesis of 4-(2-hydroxynaphthylazo) benzoic acid (H_2L^2)

Analogous synthetic procedure was followed as in case of H_2L^1 where *para*-amino benzoic acid was used in place of *ortho*-amino benzoic acid. A red crystalline product was obtained. Yield: 8.1 g, 76.05%; m.p.: 290–295 °C. Anal. calcd. for $\text{C}_{17}\text{H}_{12}\text{N}_2\text{O}_3$: C, 69.86; H, 4.14; N, 9.58%. Found: C, 69.8; H, 4.17; N, 10.15%. UV-visible (DMF) λ_{max} (nm): 251, 375, 483. IR (KBr, cm^{-1}): 3372 $\nu(\text{OH})$, 1716 $\nu(\text{COO})_{\text{asy}}$, 1448 $\nu(\text{N}=\text{N})$, 1257 $\nu(\text{C}-\text{O})$. ^1H NMR (DMSO- d_6 , 400.13 MHz) δ_{H} : 15.85 [s, 1H, OH], 8.36 [d, 1H, H-9, $J = 8.4$ Hz], 8.04 [d, 2H, H-3', H-5', $J = 8.4$ Hz], 7.86 [d, 1H, H-4, $J = 9.6$ Hz], 7.78 [d, 2H, H-2', H-6', $J = 8.4$ Hz], 7.67 [d, 1H, H-6, $J = 7.6$ Hz], 7.56 [t, 1H, H-8, $J = 7.6$ Hz], 7.43 [t, 1H, H-7, $J = 7.6$ Hz], 6.72 [d, 1H, H-3, $J = 9.6$ Hz] ppm; Signal due to $-\text{COOH}$ could not be detected due to solvent exchange. ^{13}C NMR (DMSO- d_6 , 100.62 MHz) δ_{C} : 175.95 [COO], 166.66 [C-2], 146.38 [C-1'], 142.08 [C-1], 132.57 [C-4], 130.95 [C-2', C-6'], 130.01 [C-4'], 129.34 [C-10], 129.02 [C-5], 127.92 [C-8, C-9], 126.63 [C-7], 125.37 [C-6], 121.59 [C-3], 117.11 [C-3', C-5']. The ligand skeleton and numbering scheme for ligands H_2L^1 and H_2L^2 are shown in Scheme 1.

2.2.3. Synthesis of Me_3SnHL^1 (**1**)

Trimethyltin (IV) compound **1** was synthesized by the reaction of 2-(2-hydroxynaphthylazo) benzoic acid (H_2L^1) with tri-methyl tin (IV) chloride using triethylamine as base under reflux condition with (1:1) molar ratio. In this procedure, the ligand (0.733 g, 2.059 mmol) was dissolved in 30 mL anhydrous methanol in a round bottom flask and then triethylamine base (0.2537 g, 2.509 mmol) was added dropwise and was refluxed on an oil bath for about 30 min with an equipped water cooled condenser. Trimethyltin (IV) chloride (0.5 g, 2.509 mmol) was then added to the above solution with continuous stirring and was again refluxed for about 6 h. The reaction mixture was then filtered and the precipitate containing $\text{Et}_3\text{N}\cdot\text{HCl}$ was filtered off, the filtrate was then collected and evaporated to dryness and further purification was done by hexane to get the pure red crystalline product. The crystalline product was then recrystallized in anhydrous methanol to obtain pure red crystals of complex **1**. Yield: 0.49 g, 71%; m.p.: 226–227 °C. Anal. Calcd. for $\text{C}_{40}\text{H}_{40}\text{N}_4\text{O}_6\text{Sn}_2$: C, 52.78; H, 4.43; N, 6.16%. Found: C, 52.67; H, 4.32; N, 6.13%. UV-visible (DMF) λ_{max} (nm): 287, 366, 478. IR (KBr, cm^{-1}): 3449 $\nu(\text{OH})$, 2920 $\nu(\text{C}-\text{H str. of Sn-CH}_3)$, 1632 $\nu(\text{COO})_{\text{asy}}$, 1476 $\nu(\text{N}=\text{N})$, 1443 $\nu(\text{COO})_{\text{sym}}$, 1185 $\nu(\text{C}-\text{O})$, 664 $\nu(\text{Sn}-\text{C})$, 490 $\nu(\text{Sn}-\text{O})$. ^1H NMR (CDCl_3 , 400.13 MHz) δ_{H} , Ligand skeleton: 8.43 [d, 1H, H-9, $J = 8.0$ Hz], 8.28 [d, 1H, H-3', $J = 8.4$ Hz], 8.12 [dd, 1H, H-6, $J = 8$ Hz and 1.6 Hz], 7.60–7.56 [m, 2H, H-4, H-4'], 7.51–7.46 [m, 2H, H-6', H-8], 7.36 [t, 1H, H-5', $J = 7.6$ Hz], 7.16 [t, 1H, H-7, $J = 7.6$ Hz], 6.67 [d, 1H, H-3 $J = 9.6$ Hz]; Sn- CH_3 Skeleton: 0.74 [s, 9H,



2-(2-hydroxynaphthylazo) benzoic acid (H_2L^1) 4-(2-hydroxynaphthylazo) benzoic acid (H_2L^2)

Scheme 1. The ligand skeleton and numbering scheme of ligands H_2L^1 and H_2L^2 .

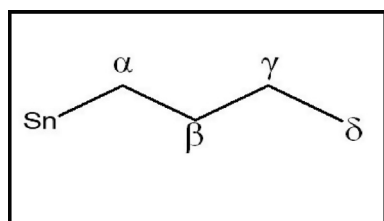
(Sn-CH₃) ²J [¹¹⁹Sn-¹H (57.2 Hz)] ppm. ¹³C NMR (CDCl₃, 100.62 MHz) δ_C: Ligand skeleton: 179.3 [COO], 171.60 [C-2], 144.2 [C-1'], 141.82 [C-1], 134.30 [C-4], 133.27 [C-4'], 132.52 [C-5'], 129.10 [C-3'], 128.74 [C-10], 128.42 [C-5], 127.49 [C-6], 126.47 [C-8], 125.87 [C-9], 124.06 [C-7], 122.37 [C-6'], 119.5 [C-3], 116.34 [C-2']; Sn-CH₃ Skeleton: -1.709 [Sn-CH₃] ppm. ¹¹⁹Sn NMR (CDCl₃, 149.18 MHz): +139.63 ppm. The other triorganotin (IV) complexes were prepared following the analogous procedure which was described above by reacting appropriate triorganotin (IV) chlorides and azo ligands.

2.2.4. Synthesis of Me₃SnHL² (2)

The tri-methyl tin (IV) compound **2** was synthesized by reacting the ligand 4-(2-hydroxynaphthylazo) benzoic acid (H₂L²) with tri-methyl tin (IV) chloride using triethylamine as a base under refluxing condition with (1:1) molar ratio to produce red crystalline compound. Yield: 0.57 g, 83.2%; m.p.: 221–222 °C. Anal. Calcd. for C₂₀H₂₀N₂O₃Sn: C, 52.78; H, 4.43; N, 6.16%. Found: C, 52.64; H, 4.27; N, 5.95%. UV-visible (DMF) λ_{max} (nm): 305, 366, 484. IR (KBr, cm⁻¹): 3443 ν(OH), 2923 ν(C-H str. of Sn-CH₃), 1595 ν(COO)_{asy}, 1498 ν(N=N), 1440 ν(COO)_{sym}, 1160 ν(C-O), 671 ν(Sn-C), 485 ν(Sn-O). ¹H NMR (CDCl₃, 400.13 MHz) δ_H: Ligand skeleton: 8.47 [d, 1H, H-9, J = 8.4 Hz], 8.14 [d, 2H, H-3', H-5', J = 7.2 Hz], 7.68–7.65 [m, 3H, H-4, H-2', H-6'], 7.56–7.52 [m, 2H, H-6, H-8], 7.38 [t, 1H, H-7, J = 7.6 Hz], 6.75 [d, 1H, H-3, J = 9.6 Hz]; Sn-CH₃ Skeleton: 0.66 [s, 9H (Sn-CH₃)] ²J [¹¹⁹Sn-¹H (57.2 Hz)] ppm. ¹³C NMR (CDCl₃, 100.62 MHz) δ_C: 176.95 [COO-], 170.97 [C-2], 146.43 [C-1'], 141.85 [C-1], 133.50 [C-4], 131.87 [C-2', C-6'], 130.88 [C-4'], 129.45 [C-10], 129.32 [C-5], 128.85 [C-8], 128.27 [C-9], 126.53 [C-7], 125.93 [C-6], 122.10 [C-3], 116.98 [C-3', C-5']; Sn-CH₃ skeleton: -4.124 [Sn-CH₃], ¹J [¹¹⁹Sn-¹³C (197.5 Hz)] ppm. ¹¹⁹Sn NMR (CDCl₃, 149.18 MHz): +139.72 ppm.

2.2.5. Synthesis of Bu₃Sn HL¹ (3)

Tri-butyl tin (IV) compound **3** was synthesized by reacting the ligand 2-(2-hydroxynaphthylazo) benzoic acid (H₂L¹) with tri-butyl tin (IV) chloride using triethylamine base under refluxing condition in (1:1) molar ratio to obtain deep red crystalline product. Yield: 0.64 g, 60.3%; m.p.: 71–72 °C. Anal. Calcd. for: C₁₁₆H₁₅₂N₈O₁₂Sn₄: C, 59.92; H, 6.59; N, 4.82%. Found: C, 60.23; H, 6.71; N, 4.78%. UV-visible (DMF) λ_{max} (nm): 287, 366, 480. IR (KBr, cm⁻¹): 2951 ν(C-H str. of ⁿBu), 1626 ν(COO)_{asy}, 1435 ν(N=N), 1343 ν(COO)_{sym}, 1151 ν(C-O), 665 ν(Sn-C), 497 ν(Sn-O). ¹H NMR (CDCl₃, 400.13 MHz) δ_H: Ligand skeleton: 8.43 [d, 1H, H-9, J = 8.0 Hz], 8.27 [d, 1H, H-3', J = 8.4 Hz], 8.10 [dd, 1H, H-6, J = 8.0 Hz and 1.2 Hz], 7.59–7.55 [m, 2H, H-4, H-4'], 7.51–7.46 [m, 2H, H-6, H-8], 7.35 [t, 1H, H-5', J = 7.6 Hz], 7.17 [t, 1H, H-7, J = 7.6 Hz], 6.66 [d, 1H, H-3 J = 9.6 Hz]; Sn-ⁿBu Skeleton: 1.71 [m, 6H, H-α], 1.48 [m, 6H, H-β], 1.39 [m, 6H, H-γ], 0.92 [t, 9H, H-δ] ppm. ¹³C NMR (CDCl₃, 100.62 MHz) δ_C: 179.50 [COO], 170.85 [C-2], 144.22 [C-1'], 141.64 [C-1], 134.34 [C-4], 133.15 [C-4'], 132.49 [C-5'], 130.95 [C-3'], 129.06 [C-10], 128.72 [C-5], 128.45 [C-6], 127.50 [C-8], 126.44 [C-9], 124.01 [C-7], 122.36 [C-6'], 119.45 [C-3], 116.34 [C-2'] Sn-ⁿBu Skeleton: 27.91 [C-β] ²J [¹¹⁹Sn-¹³C (19 Hz)], 27.09 [C-γ] ³J [¹¹⁹Sn-¹³C (65.1 Hz)], 16.99 [C-α] ¹J [¹¹⁹Sn-¹³C (342.7 Hz)], 13.68 [C-δ] ppm. ¹¹⁹Sn NMR (CDCl₃, 149.18 MHz): +126.53 ppm. The numbering scheme of Sn-Bu skeletal in the given complex is shown below (Scheme 2).



Scheme 2. The numbering scheme in SnBu skeletal.

2.3. Crystallographic data collection and structure refinement

Single crystal X-ray diffraction data were collected by the ω-scan technique using MoK_α (λ = 0.71073 Å) radiation. The **1** crystal was studied at 100 K using a RIGAKU XtaLAB Synergy, Dualflex, Pilatus 300 K diffractometer [24] with Photon Jet micro-focus X-ray Source and **2**, **3**, H₂L² at room temperature using a Bruker AXS Smart APEX-II CCD diffractometer [25]. Data collection, cell refinement, data reduction and absorption correction were carried out using CrysAlis PRO software [24] for **1** with the SMART and SAINT-PLUS [26] for **2**, **3**, H₂L². The crystal structures were solved by using direct methods with the SHELXT 2018/2 program [27]. Atomic scattering factors were taken from the International Tables for X-ray Crystallography. Positional parameters of non-H-atoms were refined by a full-matrix least-squares method on F² with anisotropic thermal parameters by using the SHELXL 2018/3 program [28]. All hydrogen atoms were placed in calculated positions (C-H = 0.93–0.98 Å) and included as riding contributions with isotropic displacement parameters set to 1.2–1.5 times the U_{eq} of the parent atom. In **3**, a model of disorder of *n*-butyl groups was proposed. Crystal data and structure refinement parameters are shown in Table S1, while selected geometric parameters are collected in Tables 2, 3 and S2.

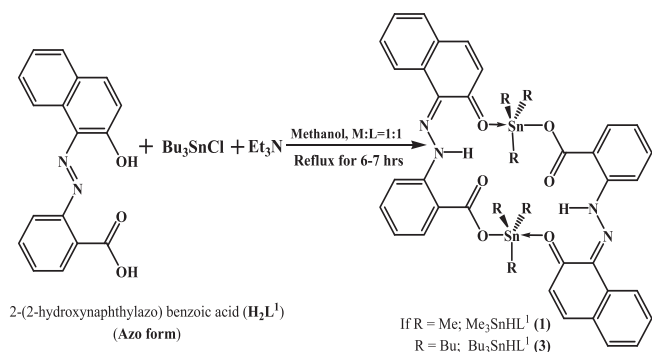
2.4. Antimicrobial assay

The antimicrobial screening of the compounds **1–3** and ligands were performed following modified Kirby-Bauer-Diffusion Assay [29]. Three bacterial species (*Escherichia coli*, *Pseudomonas auriginosa* and *Staphylococcus aureus*) and three species of fungi (*Fusarium verticilloides*, *Fusarium chlamydosporum* and *Fusarium oxysporum*) were employed for the assay. Prior to the assay all the test organisms were revived by streaking on respective agar media plates. For preparing bacterial inoculums, fresh culture was inoculated in nutrient broth and incubated for 24 h at 37 °C and diluted up to 10⁻⁴ using sterile water. For preparing fungal inoculums, 7-days old fungal culture was used, 5 mL of sterile distilled water was added to the vials containing the fungal cultures. The colonies were gently scraped out along with water and the suspension was vortexed at a minimum speed and used directly as inoculums. Filter paper discs of 6 mm diameter were prepared from Whatman No.1 and sterilized by autoclaving prior to the assay. A thin layer of bacterial culture was prepared using an L-spreader on the surface of Tomato Juice Agar (TJA) medium plates by inoculating 150 μL of bacterial cell suspension. For fungal culture, Rojo Congo Agar (RCA) medium plates were inoculated with 150 μL of fungal spore suspension (diluted to 10⁻⁵). A manual rotary plate spreader was used for a proper and uniform layer of bacteria and fungi on their respective media plates. The plates were allowed to dry for about 1 min inside the laminar air flow chamber. Filter paper disc previously saturated with test sample solutions (1 mg/mL) for screening test and for quantitative assay, different doses (25, 50, 100, 200, 500 μg/mL) were placed on the surface of the bacterial/fungal culture. Standard antibiotic discs of Streptomycin (1 mg/mL) and Fluconazole (1 mg/mL) were used against the test bacteria and fungi for comparison with the test samples. All tests were performed in triplicate and mean values are presented. The plates were incubated for 24 h at 37 °C for bacteria and 72 h at 30 °C for fungi. The bacterial and fungal inhibition zones (mm) were recorded for all samples as well as for the standard antibiotics.

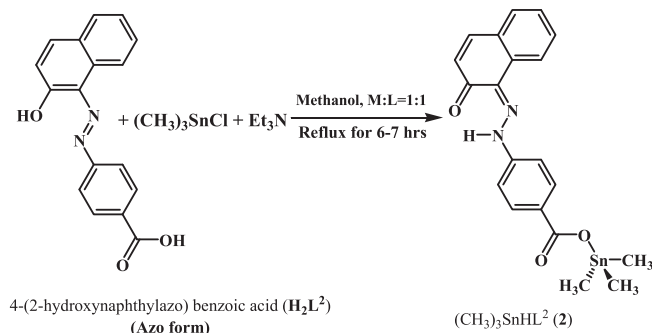
3. Results and discussion

3.1. Synthesis

Triorganotin (IV) complexes **1–3** were synthesized by reacting 2/4-(2-hydroxynaphthylazo) benzoic acids (H₂L¹⁻²) with appropriate triorganotin (IV) chlorides [R = Me (**1** and **2**), Bu (**3**)] using anhydrous methanol in presence triethylamine base in 1:1 stoichiometric molar



Scheme 3. Reaction scheme for the synthesis of compounds 1 and 3.



Scheme 4. Reaction scheme for the synthesis of compound 2.

ratio. The complexes were obtained in good yield and were found to be soluble in all common organic solvents. The reaction schemes for the synthesis of complexes 1 and 3 are shown in Scheme 3 and for complex 2 in Scheme 4.

3.2. Spectroscopic characterization

3.2.1. UV-spectroscopy

The UV-visible spectra of the ligands (H_2L^{1-2}) and compounds (1–3) were recorded in DMSO and chloroform solution (10^{-4} M) respectively at room temperature. The electronic spectra of H_2L^1 and H_2L^2 showed UV absorption peaks at 251–252 and 315–316 nm which may be assigned to $\pi \rightarrow \pi^*$ transition of aromatic ring and $n \rightarrow \pi^*$ transition of carboxylic acid group respectively [19]. The UV-visible spectra for compounds 1–3 exhibited three absorption bands at 287–306, 366 and 478–487 nm respectively. After coordination, $\pi \rightarrow \pi^*$ and $n \rightarrow \pi^*$ transitions were observed at slightly higher wavelength in the complexes. The new bands observed at 478–487 nm indicate ligand to metal charge transfer [19,30]. The slight increase of the λ_{max} value from the ligand to the organotin (IV) complexes indicates the coordination of the ligand to tin atom.

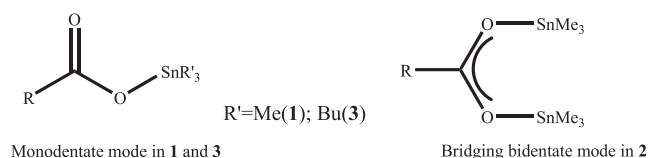
3.2.2. IR spectroscopy

The IR spectroscopic data for azo-carboxylate ligands H_2L^{1-2} and compounds 1–3 are given in the experimental section. The O–H stretching absorption band for the free azo-carboxylate ligands (H_2L^1 and H_2L^2) was found in the region 3300 – 3400 cm^{-1} . The asymmetric [$\nu_{asym}(\text{COO})$] stretching frequencies of the ligands H_2L^1 and H_2L^2 were observed at 1710 and 1716 cm^{-1} respectively and in the complexes, these bands were shifted to lower frequencies at 1625 – 1632 cm^{-1} . The shifting of the absorption bands of these complexes relative to the free carboxylate ligands indicates the carboxylate coordination to Sn-atom [16]. The IR absorption bands observed at 530 – 680 cm^{-1} and 450 – 500 cm^{-1} in the complexes are assigned for Sn–C and Sn–O respectively [21,31]. Further, useful information about mode of coordination of carboxylate group with the Sn-centre can also be

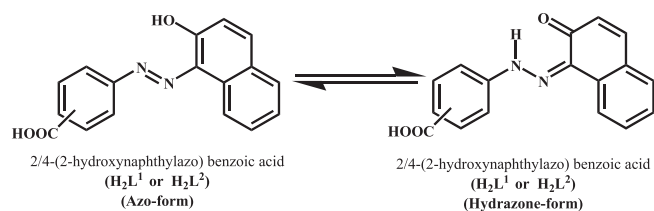
determined from the study of IR stretching frequency of carboxylate group [29]. In general, carboxylate exhibits two types of bands, strong asymmetric stretching band, [$\nu_{asym}(\text{COO})$] observed near 1580 – 1650 cm^{-1} and a weaker symmetric stretching band, [$\nu_{sym}(\text{COO})$] near 1320 – 1450 cm^{-1} . Moreover, if the value of $\Delta\nu$ [$\nu_{asym}(\text{COO}) - \nu_{sym}(\text{COO})$] is below 200 cm^{-1} indicates bi-dentate mode of coordination while if the value of $\Delta\nu$ is greater than 200 cm^{-1} is an indicative of the presence of mono-dentate mode of coordination of the carboxylate ligands to the tin in the complexes [20,32]. In complexes 1 and 3, the characteristic asymmetric stretching frequency bands were observed at 1632 cm^{-1} and 1626 cm^{-1} while the symmetric stretching frequency bands were observed at 1345 cm^{-1} in and 1343 cm^{-1} and the value of $\Delta\nu$ was found to be 287 cm^{-1} and 283 cm^{-1} respectively. Thus it can be concluded that in both the complexes 1 and 3, carboxylate ligand coordinate in mono-dentate mode of coordination to the Sn-centre [17]. Furthermore, in case of complex 2, the similar asymmetric IR stretching frequency band was observed at 1625 cm^{-1} while the symmetric stretching frequency band was observed at 1440 cm^{-1} and the value of $\Delta\nu$ was found to be 185 cm^{-1} . This implies that the complex 2 is in bi-dentate bridging mode of coordination of carboxylate ligand to the Sn-centre [19,32]. The mode of coordination of carboxylate ligands in these complexes were found to be in consistent with the crystal structures of the complexes (*vide infra*). The coordination mode of the carboxylate ligands in the complexes are shown in Scheme 5.

3.2.3. Multinuclear (1H , ^{13}C and ^{119}Sn) NMR spectroscopy

1H , ^{13}C NMR spectral data of the ligands (H_2L^1 and H_2L^2) were recorded in DMSO- d_6 while 1H , ^{13}C and ^{119}Sn NMR spectral data for the complexes 1–3 were recorded in $CDCl_3$ and the data are provided in the experimental section while some spectra for the ligands and complexes are also provided as the Electronic Supplementary Information (ESI). The complete assignments of 1H , ^{13}C NMR spectra of the ligands were accomplished by examining their chemical shift values, integration values, multiplicity patterns and also by interpretation of their correlated spectroscopy (1H - 1H COSY). These data was also examined by comparing the proton NMR spectral data of similar type of azo-ligands derived from either *o/p*-amino benzoic acids or β -naphthol reported earlier [17,22,33–35]. The assignments of the chemical shift position of the protons for the complexes were achieved by inferring the conclusions which were drawn from the ligand assignments owing to the similarity of their spectral data. The aromatic protons of the azo ligands H_2L^1 and H_2L^2 were observed in the range 6.38–8.37 ppm whereas the aromatic protons in all the complexes 1–3 were observed in the range 6.66–8.47 ppm. In complex 1 and 2, a singlet peak was observed at 0.74 ppm and 0.66 ppm respectively which can be assigned to tin-methyl protons. In complex 3, a triplet and three multiplet peaks were observed at 0.92 ppm and 1.39–1.71 ppm due to methyl and three methylene protons of tri-butyltin moiety. The ^{13}C NMR spectra of the azo ligands H_2L^1 and H_2L^2 showed $\delta(\text{COO})$ signals at 178.94 and 175.95 ppm respectively, but in case of all the complexes 1–3, the $\delta(\text{COO})$ signals were observed in the range 176–179 ppm. The ^{13}C NMR signals for aromatic ring carbons of the free azo ligands H_2L^1 and H_2L^2 were observed at the range 116.12–178.94 ppm whereas in case of complexes 1–3, the corresponding values were found in the range 116.34–179.50 ppm. The number of ^{13}C NMR signals observed in the ligands and the complexes were found to be in good agreement with the



Scheme 5. Coordination mode of carboxylate ligands in complexes 1–3.



Scheme 6. Azo and hydrazone tautomeric forms of azo-carboxylate ligands H_2L^1 and H_2L^2 .

expected number of signals. The azo-carboxylate ligands H_2L^1 and H_2L^2 which contain an OH group at the *ortho*-position to the azo linkage can lead to tautomerize to give two tautomeric structures, azo and hydrazone forms. In solution state these two isomeric forms remain in equilibrium as shown in Scheme 6.

However, due to rapid exchange process at room temperature we could not observe different resonances for the two tautomers in solution. For the identification of position of the azo-hydrazone equilibrium, we have used the ^{13}C NMR chemical shift values of naphthalene ring carbon, C-2 for the estimation of the relative tautomeric population as calculated in case of 1-phenylazo-2-naphthol derivatives [35,36]. A strong electron withdrawing group present in the *para* position of phenyl ring can shift the equilibrium almost completely to the hydrazone form with a C-2 chemical shift of approximately 180 ppm [33], while the corresponding value for azo form was found by additivity rule to be approximately 147 ppm [36,37]. Due to the structural similarity of our azo-carboxylate ligands H_2L^1 and H_2L^2 with the azo ligands with β -naphthol reported earlier [32], we calculated equilibrium constants for the tautomeric proton exchange reaction using the following Eq. (1) [34].

$$K_{\text{azo-hydrazone}} = \frac{[\text{Hydrazone}]}{[\text{azo}]} = \frac{\delta_{C2} - 147 \text{ ppm}}{180 \text{ ppm} - \delta_{C2}} \quad (1)$$

The equilibrium constant of the ligands calculated by using Eq. (1) are listed in Table 1.

For complexes, the geometry and coordination number around tin centers in solution state can be determined using 2J ($^{119/117}Sn-^1H$) and nJ ($^{119}Sn-^{13}C$) coupling constants [17,19,38–40]. In complexes 1 and 2, the 2J ($^{119}Sn-^1H$) coupling constant values were found to be 57.2 Hz indicating 4-coordinate tetrahedral geometry of Sn-centre in both the complexes [17,19,38–41]. Furthermore, four coordinate tetrahedral geometry of the complexes were also determined by measuring the nJ ($^{119}Sn-^{13}C$) coupling constant values. It is generally observed that four coordinate tributyltin compounds exhibit couplings 1J ($^{119}Sn-^{13}C$) in the range of 325–390 Hz and five coordinated complexes in the range of 430–540 Hz [17,19,38–41]. In complex 3, the 1J ($^{119}Sn-^{13}C$), 2J ($^{119}Sn-^{13}C$) and 3J ($^{119}Sn-^{13}C$) coupling satellites were observed at 342.7 Hz, 19 Hz and 65.1 Hz respectively which indicate the four coordinate tetrahedral geometry of the tin centre for the complex in solution state [19,21,38]. In addition, using Lockhart and Mander's equation [39] $\{\theta(C-Sn-C) = 0.0161 | ^2J(Sn-H) |^2 - 1.32 | ^2J(Sn-H) | + 133.4\}$, the angle between C-Sn-C in complexes 1 and 2 were calculated and found to be 110.56° for both the complexes indicating the four coordinated tetrahedral geometry [21,38]. The geometry of the complexes was further confirmed by ^{119}Sn NMR spectral study. The ^{119}Sn NMR spectra for the complexes 1 and 2 were observed at +139.63 ppm and

Table 1

The equilibrium constants of azo ligands H_2L^1 and H_2L^2 in DMSO- d_6 calculated from ^{13}C NMR chemical shifts of C-2 using Eq. (1).

Azo ligands	δ_{C2} /ppm (in DMSO- d_6)	$K_{\text{azo-hydrazone}}$
H_2L^1	167.43	1.625
H_2L^2	166.66	1.47

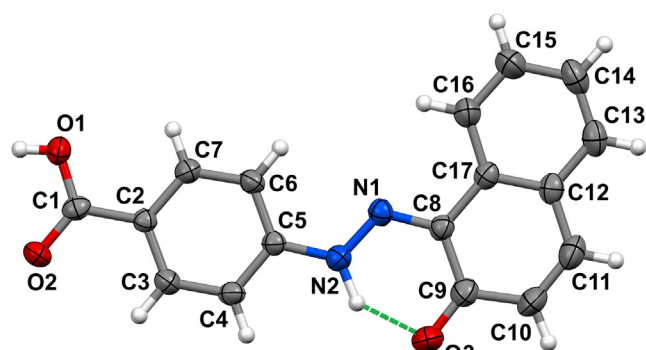


Fig. 1. View of the H_2L^2 molecule showing the atom-labeling scheme. Displacement ellipsoids are drawn at 50% probability level.

+139.72 ppm respectively. For complex 3 the sharp signal of ^{119}Sn resonance was observed at +126.53 ppm. These resonances of the complexes 1–3 suggest the four coordinate tetrahedral geometry in solution state [21,38–41].

3.3. X-ray crystal structure description

3.3.1. Crystal structure of H_2L^2

The ORTEP image of the free acid (H_2L^2), belonging to the $C2/c$ space group, is shown in Fig. 1. The molecule is approximately planar with no twist about the central C=N=N-C bonds linking the aromatic rings, as indicated by the torsion angles $N1-N2-C5-C6 = 0.8(5)^\circ$ and $N2-N1-C8-C9 = -0.2(5)^\circ$. This can be rationalized by the formation of intramolecular hydrogen bond $N2-H2A...O3$, which additionally stiffens the entire molecule. The carboxylic acid group is coplanar with its parent phenyl ring [$O(1)-C(1)-C(2)-C(3) = -178.7(3)^\circ$]. The carboxylic acid H-atom forms an intramolecular hydrogen bond, $O1-H1A...O2^{#1}$ [#1:1-x,-1-y,1-z], with the O-atom from neighboring carboxylic acid group (Table 2). This causes, that the crystal packing (Fig. S7) features centrosymmetrically related dimers associate via the eight-membered carboxylic acid dimer synthon $\{\dots HOC(=O)\}_2$, which can be described by graph set notation as $R_2^2(8)$ [43].

3.3.2. Crystal structure of complex 1

The molecular structure of 1 is shown in Fig. 2. Selected bond distances and angles are listed in Table 3. The complex 1 is a cyclic centrosymmetric dimer. The geometry around the five-coordinated Sn atom is distorted trigonal bipyramidal, in which three methyl groups occupying the equatorial positions with almost identical bond distances

Table 2

Hydrogen bonding parameters for the ligand (H_2L^2) and the triorganotin(IV) complexes 1, 2 and 3.

Compound	D-H...A	d(D-H)	d(H...A)	d(D...A)	<(DHA)
H_2L^2	O(1)-H(1A)...O(2) ^{#1}	0.82	1.84	2.642(3)	164.2
	N(2)-H(2A)...O(3)	1.02(4)	1.68(4)	2.547(4)	139(3)
1	N(1)-H(1)...O(2)	0.84(2)	2.08(2)	2.693(2)	130(2)
	N(1)-H(1)...O(3)	0.84(2)	2.03(2)	2.650(2)	130(2)
2	C(2)-H(2C)...O(2) ^{#2}	0.98	2.36	3.189(2)	146.0
	C(4)-H(14)...O(3) ^{#3}	0.93	2.53	3.382(1)	151.7
3	N(1)-H(1A)...O(3)	0.85(2)	1.81(1)	2.555(1)	146(2)
	N(2)-H(2A)...O(1)	0.86	2.06	2.694(2)	129.5
	N(2)-H(2A)...O(2)	0.86	2.07	2.691(2)	128.3
	N(4)-H(4A)...O(4)	0.86	2.10	2.717(2)	128.6
	N(4)-H(4A)...O(5)	0.86	2.02	2.657(2)	129.9
	N(6)-H(6)...O(7)	0.86	2.09	2.706(2)	128.4
	N(6)-H(6)...O(8)	0.86	2.03	2.662(2)	129.9
	N(8)-H(8)...O(10)	0.86	2.08	2.690(2)	127.2
N(8)-H(8)...O(11)	0.86	2.04	2.672(2)	130.1	

Symmetry code: (#1) 1-x,-1-y,1-z; (#2) 1-x,1-y,1-z; (#3) 2-x,-y,1-z.

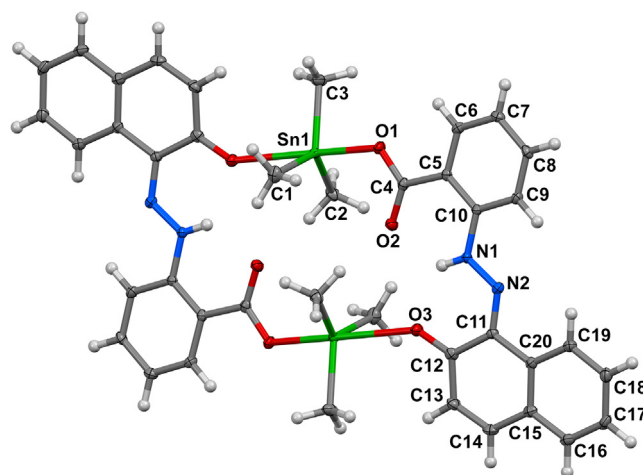


Fig. 2. The molecular structure of **1**. Displacement ellipsoids drawn at 50% probability level.

[mean bond length Sn-C = 2.121(2)Å] and the axial positions being filled by a carboxylate oxygen and a phenoxide oxygen of an adjacent molecule. The Sn-C bond lengths are consistent with those reported in the literature [42–44]. The C-Sn-C bond angles (C1-Sn1-C2, C1-Sn1-C3, C2-Sn1-C3) are 126.63(9)°, 118.86(9)° and 110.79(8)°, respectively and their sum is 356.28(9)°. Whereas, two oxygen atoms are bonded asymmetrically to Sn atom with significantly different Sn-O distances of 2.127(1)Å and 2.616(2)Å respectively. Longer weak Sn-O bond should rather be considered as secondary interactions but nevertheless with a physical meaning. The literature search showed that for apical Sn-O bonds with monodentate ligands, in pentacoordinated compound of Sn such bonds are reported [45]. The O1-Sn1-O3^{#2} [#2: 1-x, 1-y, 1-z], bond angle is 174.62(5)°. The asymmetrical arrangement of oxygen atoms causes significant deformations of the Sn coordination sphere. The deformation of the Sn coordination sphere can be explained by the Berry pseudorotation mechanism [46] and characterized quantitatively by parameter τ defined by Addison et al. [47], ($\tau = 0.80$; cf. the τ values for the idealized geometries are $\tau = 0$, square planar, $\tau = 1$, trigonal bipyramidal). An intramolecular N-H...O hydrogen bonds [N1-H1...O2 and N1-H1...O3] help to establish near planar conformation of molecule (Table 2). Packing diagrams of complex **1** are shown in Fig. S8a-b.

3.3.3. Crystal structure of complex 2

The molecular structure of complex **2** is shown in Fig. 3. Selected bond lengths and bond angles are presented in Table 3. The compound **2** forms in solid state an infinite zig-zag 1-D chain structure connected by bridging carboxylate coordination to tin ions. The bond distances are

Table 3
Selected bond lengths (Å) and bond angles (°) for the organotin (IV) complexes.

Atoms	1 Bond Length (Å)	Atoms	2 Bond Length (Å)	Atoms	3 Bond Length (Å)
Sn(1)-O(1)	2.1273(13)	Sn(1)-O(1)	2.178(7)	Sn(1)-O(3)	2.116(11)
Sn(1)-O(3) ^{#1}	2.6161(15)	Sn(1)-O(2) ^{#2}	2.353(7)	Sn(1)-O(4)	2.721(11)
Sn(1)-C(1)	2.118(2)	Sn(1)-C(18)	2.236(9)	Sn(1)-C(18)	2.18(2)
Sn(1)-C(2)	2.111(2)	Sn(1)-C(19)	2.117(12)	Sn(1)-C(22)	2.22(3)
Sn(1)-C(3)	2.133(2)	Sn(1)-C(20)	2.121(12)	Sn(1)-C(26)	2.18(2)
O(1)-Sn(1)-C(1)	96.04(7)	O(1)-Sn(1)-C(18)	99.2(3)	O(3)-Sn(1)-C(18)	100.2(6)
O(1)-Sn(1)-C(2)	103.05(7)	O(1)-Sn(1)-C(19)	86.3(4)	O(3)-Sn(1)-C(22)	90.8(6)
O(1)-Sn(1)-C(3)	89.41(7)	O(1)-Sn(1)-C(20)	94.0(4)	O(3)-Sn(1)-C(26)	98.3(8)
O(1)-Sn(1)-O(3) ^{#1}	174.62(5)	O(1)-Sn(1)-O(2) ^{#2}	175.3(3)	O(3)-Sn(1)-O(4)	174.8(4)
C(1)-Sn(1)-C(2)	126.63(9)	C(18)-Sn(1)-C(19)	119.6(4)	C(18)-Sn(1)-C(22)	115.7(9)
C(1)-Sn(1)-C(3)	118.86(9)	C(18)-Sn(1)-C(20)	121.4(4)	C(18)-Sn(1)-C(26)	127.0(9)
C(2)-Sn(1)-C(3)	110.79(8)	C(19)-Sn(1)-C(20)	118.0(5)	C(22)-Sn(1)-C(26)	113.3(10)

Symmetry code: (#1) 1-x, -1-y, 1-z; (#2) 3/2-x, -1/2 + y, 3/2-z.

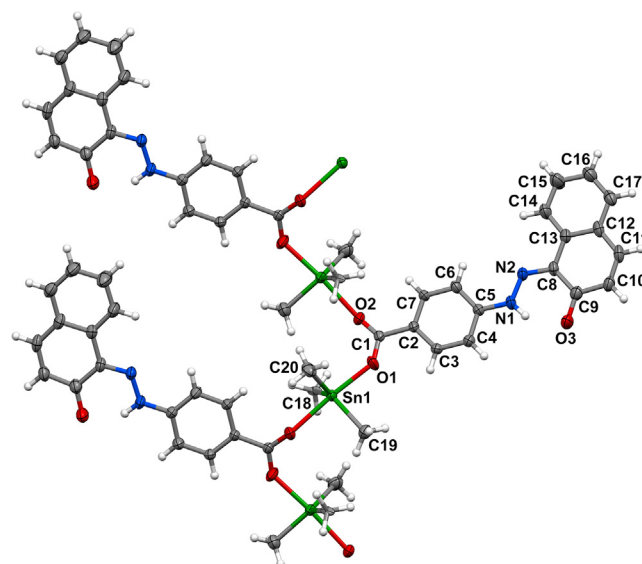


Fig. 3. The 1-D infinite zigzag chain of **2**. Displacement ellipsoids are drawn at 50% probability level.

Sn-O1 = 2.177(8)Å and Sn-O2^{#2} = 2.352(7)Å respectively. The two O atoms are to a lesser extent bonded asymmetrically to tin atom than in **1**. Like in **1** the coordination geometry of the tin center is a slightly distorted trigonal bipyramid, thus the Sn atom is five-coordinated with the two oxygen atoms occupying the axial sites [the O-Sn-O axial angle is O1-Sn1-O2^{#2} = 175.3(3)°, #2: 3/2-x, -1/2 + y, 3/2-z]. Three Sn-methyl groups define the equatorial plane, and the sum of the trigonal C-Sn-C angles is 359.0° which indicates that the three methyl groups and tin atoms are nearly coplanar. The value of parameter $\tau = 0.90$ confirms the 5-coordinated distorted trigonal bipyramidal geometry of Sn.

The molecules additionally stabilize an intramolecular N-H...O hydrogen bonds (Table 2). The molecular packing of compound **2** is shown in Fig. S9.

3.3.4. Crystal structure of complex 3

In crystals of compound **3** (Fig. 4), which crystallizes in $P2_1$ space group, there are two symmetry independent molecules in the asymmetric unit. Selected bond lengths and bond angles are presented in Table 3. In contrast to **1**, both molecules form non-centrosymmetric dimers. The atomic coordinates of those two independent molecules have been thoroughly tested without success for higher symmetry by means of the PLATON program [48]. Like in **1** and **2**, the geometry around the each Sn atoms is distorted trigonal bipyramidal. The parameter τ varies from 0.73 to 0.82 for Sn centers, respectively.

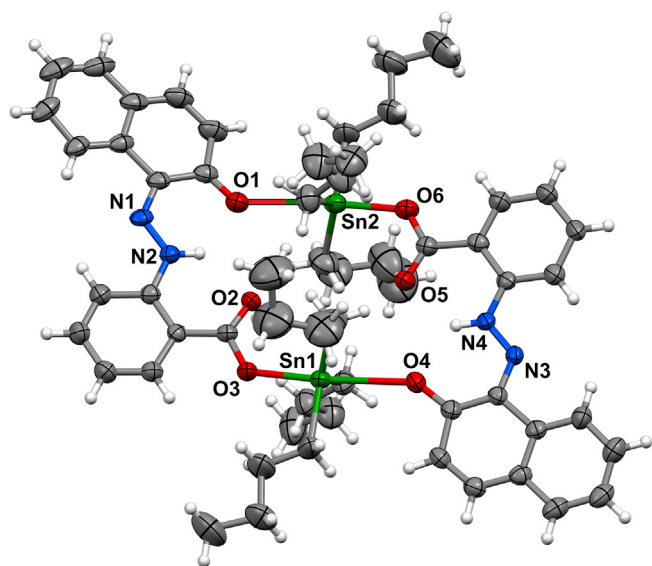


Fig. 4. The molecular structure of a dimeric unit of **3**. Displacement ellipsoids are drawn at 20% probability level.

The short Sn-O bonds vary from 2.068(13) Å to 2.117(11) Å and long Sn-O bonds vary from 2.721(11) Å to 2.814(11) Å. The coordination sphere is complemented by three disordered *n*-butyl groups lying in equatorial positions. As in case of **1** and **2**, intra-molecular hydrogen bonds of the type N–H...O (Table 2) play an important role in stabilizing the structure. The crystal packing of complex **3** is shown in Fig. S10.

3.4. Antimicrobial activity

Antimicrobial activity of the compounds and the ligands were studied by screening them against three bacteria (*E. coli*, *P. auriginosa* and *S. aureus*) and three fungi (*F. verticilloides*, *F. chlamydosporum* and *F. oxysporum*). The screening results of the antimicrobial assay of the synthesized compounds and the ligands along with the standard compounds streptomycin and fluconazole as positive control are shown in Table 4. From the table, it is seen that only compound **3** exhibited antimicrobial activity while the ligands and the compounds **1** and **2** did not show any activity. Therefore, we have performed dose dependant quantitative assay for only compound **3** against the bacterium (*S. aureus*) and the fungus (*F. oxysporum*) which exhibited significant antimicrobial activities in the screening tests along with standard antibiotic compounds streptomycin and fluconazole. The results of the

Table 4

Microbial growth inhibition properties of three compounds (1 mg/mL) against bacteria and fungi along with standard antibiotics.

Sl.No.	Test samples compounds/ antibiotics	Microbial growth inhibition zone*					
		Bacteria			Fungi		
		EC	PA	SA	FV	FC	FO
1.	1	–	–	–	–	–	–
2.	2	–	–	–	–	–	–
3.	3	–	–	+++	+	++	+++
4.	H ₂ L ¹	–	–	–	–	–	–
5.	H ₂ L ²	–	–	–	–	–	–
6.	Streptomycin	+	+	+	NT	NT	NT
7.	Fluconazole	NT	NT	NT	–	–	–

EC = *E. coli*, PA = *P. auriginosa*, SA = *S. aureus*, FV = *F. verticilloides*, FC = *F. chlamydosporum* and FO = *F. oxysporum*. [*Inhibition of microbial growth with more than 5, 10 and 15 mm are marked with '+', '++' and '+++' respectively. '–' = Not active; NT = Not tested].

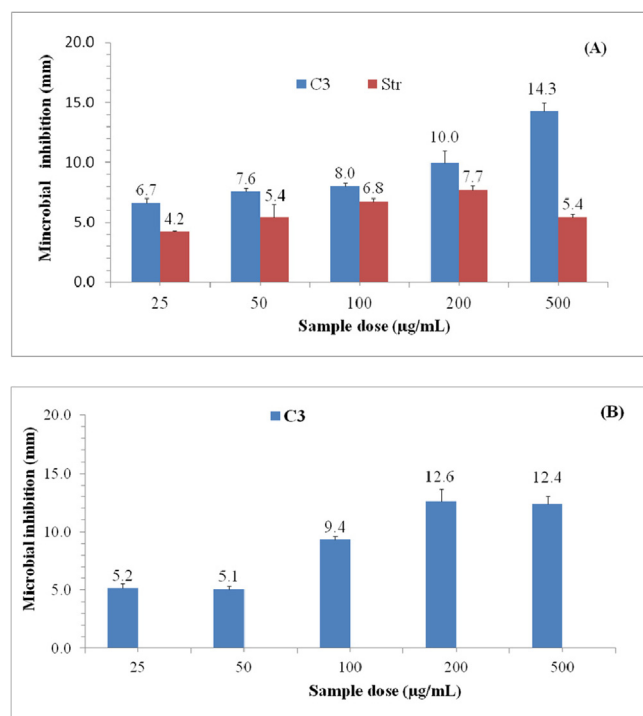


Fig. 5. Microbial growth inhibition properties at different doses of compound **3** (C3) and streptomycin (Str) against *S. aureus* (A) and *F. oxysporum* (B). T-bars on the histogram represent standard deviation of mean. Fluconazole did not show activity against the fungus *F. oxysporum*.

quantitative assay test for compound **3** and the standard antibiotics are also shown in Fig. 5. It has also been observed that, there is linear increase in the antimicrobial activity of the compound **3** with increase in their concentrations against the bacterium at different doses indicating concentration dependent activity. The antibiotic streptomycin (Str) also displayed increase in antimicrobial activity up to 200 µg/mL and decreases thereafter with the increase in the dose. However, the antimicrobial activity of the compound **3** increased significantly from 6.7 mm at 25 µg/mL to 14.3 mm at 500 µg/mL against the bacteria *S. aureus*. For fungal, the antifungal activity of the compound **3** increased significantly from 5.2 mm at 25 µg/mL to 12.6 mm at 200 µg/mL against *F. oxysporum*. It is also seen that fluconazole (FZ) did not show antifungal activity against the fungus *F. oxysporum* at all different doses.

The picture for antimicrobial assay plates for the antimicrobial activity of the compound **3** and antibiotics are also provided in Fig. S6 as supplementary material. Compound **3** is found to be the most effective antimicrobial agents against *S. aureus* and *F. oxysporum* among the tested compounds. The higher antimicrobial activity of tributyltin(IV) compound **3** as compared to its corresponding trimethyltin(IV) compounds **1** and **2** were found to be fully in consistent with the earlier reports [38,49–51].

The antimicrobial activity of the compound **3** against the bacteria *S. aureus* is found to be comparable with the related triorganotin(IV) compounds with azo- carboxylate ligands reported earlier [48]. The antimicrobial activity of compound **3** was found to exhibit higher activity than the standard antibiotics streptomycin and fluconazole.

4. Conclusions

Three triorganotin(IV) complexes **1–3** were synthesized by reacting azo-carboxylic acid ligands with triorganotin(IV) chlorides using triethylamine base. The complete characterization of the complexes was accomplished by elemental analysis, UV-Vis, IR and multinuclear NMR spectroscopy. Crystal structure of compound **2** exhibit polymeric

structure while **1** and **3** showed dimeric structures. The geometry around tin atom in all the complexes is trigonal bipyramidal geometry where three alkyl groups occupy the equatorial plane while the axial positions are being occupied by carboxylate and phenoxide oxygen atoms. Carboxylate ligands coordinate in bidentate bridging fashion in **2** while monodentate mode in **1** and **3**. The X-ray crystal structure analysis of the compounds reveal that there is intra-molecular hydrogen bonding between N–H...O in the structures. NMR spectral studies suggest 4-coordinate geometry of all the complexes in solution state. Thus, five coordinate structures of the complexes in solid state upon dissolution undergo dissociation into four coordinate species in solution. The compounds were also screened for their antimicrobial activity against few microbes and compared with standard antibiotics streptomycin and fluconazole Compound **3** showed effective antimicrobial activity against the bacteria *S. aureus* and fungal species *F. oxysporum*. Since compound **3** exhibits higher antimicrobial activity than the standard antibiotics against few microbes, this compound could be further investigated for its antimicrobial activity and could be considered as a potential candidate for antimicrobial therapeutic applications.

Declaration of Competing Interest

The authors declare that they have no known competing financial interests or personal relationships that could have appeared to influence the work reported in this paper.

Acknowledgements

Authors would like to thank SAIF, IIT Madras for providing crystal structure for compound **3**, IISc, Bangalore for NMR spectra. Authors would also like to thank DBT, Govt. of India (grant no. BT/32/NE/2011) for Biotech hub.

Appendix A. Supplementary data

Supplementary data to this article can be found online at <https://doi.org/10.1016/j.ica.2019.119172>.

References

- [1] E.R.T. Tiekink, Appl. Organomet. Chem. 5 (1991) 1.
- [2] V. Chandrasekhar, K. Gopal, P. Thillagar, Acc. Chem. Res. 40 (2007) 420.
- [3] E.R.T. Tiekink, Trends Organomet. Chem. 1 (1994) 71.
- [4] C. Ma, Z. Guo, R. Zhang, Polyhedron 27 (2008) 420.
- [5] C. Ma, J. Sun, Dalton Trans. (2004) 1785.
- [6] V. Chandrasekhar, C. Mohapatra, R.J. Butcher, Cryst. Growth Des. 12 (2012) 3285.
- [7] C. Ma, Q. Jian, R. Zhang, D. Wang, Dalton Trans. (2003) 2975.
- [8] X. Xiao, L. Yan, Z. Mei, D. Zhu, Xu Li, RSC. Adv. 4 (2014) 3096.
- [9] D. Du, Z. Jiang, C. Liu, A.M. Sakho, D. Zhu, L. Xu, J. Organomet. Chem. 696 (2011) 2549.
- [10] A.S. Sougoule, Z. Mei, X. Xiao, C.A. Balde, S. Samoura, A. Dolo, D. Zhu, J. Organomet. Chem. 758 (2014) 19.
- [11] M. Gielen, M. Biesemans, D. de Vos, R. Willem, J. Inorg. Biochem. 79 (2000) 139.
- [12] D. Tzimopoulos, I. Sanidas, A.C. Varvogli, A. Czapik, M. Gdaniec, E. Nikolakaki, P.D. Akrivos, J. Inorg. Biochem. 104 (2010) 423.
- [13] A. Rehman, M. Hussain, Z. Rehman, S. Ali, A. Rauf, F.H. Nasim, M. Helliwell, Inorg. Chim. Acta 370 (2011) 27.
- [14] D.K. Dimertzi, V. Dokouro, A. Primikiri, R. Vergas, C. Silvestru, U. Russo, M.A. Dimertzi, J. Inorg. Biochem. 103 (2009) 738.
- [15] T.S. Basu Baul, W. Rynjah, E. Rivarola, A. Lycka, M. Holcapek, R. Jirasko, D. de Vos, R.J. Butcher, A. Linden, J. Organomet. Chem. 691 (2006) 4850.
- [16] T.S. Basu Baul, K.S. Singh, A. Lycka, A. Linden, X. Song, A. Zapata, G. Eng, Appl. Organomet. Chem. 20 (2006) 788.
- [17] T.S. Basu Baul, K.S. Singh, X. Song, A. Zapata, G. Eng, A. Lycka, A. Linden, J. Organomet. Chem. 689 (2004) 4702.
- [18] T.S. Basu Baul, K.S. Singh, M. Holcapek, R. Jirasko, E. Rivarola, A. Linden, J. Organomet. Chem. 690 (2005) 4232.
- [19] M. Roy, S.S. Devi, S. Roy, C.B. Singh, K.S. Singh, Inorg. Chim. Acta 426 (2015) 89.
- [20] M. Roy, S. Roy, K.S. Singh, J. Kalita, S.S. Singh, New J. Chem. 40 (2016) 1471.
- [21] M. Roy, S. Roy, K.S. Singh, J. Kalita, S.S. Singh, Inorg. Chim. Acta 439 (2016) 164.
- [22] A. Lyc'ka, D. Lus'tinec, J. Holec'ek, M. Nádvořník, M. Holc'apek, Dyes Pigm. 50 (2001) 203.
- [23] P. Smitha, S.K. Asha, C.K.S. Pillai, J. Polym. Sci. Pol. Chem. 43 (2005) 4455.
- [24] O.D. Rigaku, CrysAlis PRO, Rigaku Oxford Diffraction Ltd, Yarnton, Oxfordshire, England, 2019.
- [25] Bruker. APEX2. Bruker AXS Inc., Madison, Wisconsin, USA, 2008.
- [26] SMART and SAINT-PLUS. Area Detector Control and Integration Software. Versions 5.629 and 6.45, Bruker Analytical X-Ray Instruments Inc., Madison, WI, USA, 2003.
- [27] G.M. Sheldrick, SHELXT – integrated space-group and crystal-structure determination, Acta Cryst. A71 (2015) 3.
- [28] G.M. Sheldrick, Crystal structure refinement with SHELXL, Acta Cryst. C 71 (2015) 3.
- [29] J. Hudzicki, Kirby-Bauer Disk Diffusion Susceptibility Test Protocol, American Society for Microbiology (<https://www.asm.org/Protocols/Kirby-Bauer-Disk-Diffusion-Susceptibility-Test-Pro>), 2009.
- [30] R.M. Maurya, M.N. Jayaswal, V.G. Puranik, P. Chakrabarti, S. Gopinathan, C. Gopinathan, Polyhedron 16 (1997) 3977.
- [31] C. Pettinari, F. Marchetti, R. Pettinari, D. Martini, A. Drozdov, S. Troyanov, Inorg. Chim. Acta 325 (2001) 103.
- [32] C. Ma, J. Li, R. Zhang, D. Wang, Inorg. Chim. Acta 359 (2006) 2407.
- [33] R. Carballo, A. Castineiras, B. Covelo, J. Niclos, E.M. Vazquez-Lopez, Polyhedron 20 (2000) 2415.
- [34] L. Racáné, Z. Mihalić, H. Cerić, J. Popović, V. Tralić-Kulenović, Dyes Pigm. 96 (2013) 672.
- [35] S.H. Alarcón, A.C. Olivieri, D. Sanz, R.M. Claramunt, J. Elguero, J. Mol. Struct. 705 (2004) 1.
- [36] A.C. Olivieri, R.B. Wilson, I.C. Paul, D.Y. Curtin, J. Am. Chem. Soc. 111 (1989) 5525.
- [37] M. Gelbcke, C. Masiala-Tsobo, F. Parmentier, R. Declerck-Grimée, Anal. Lett. 13 (1980) 975.
- [38] M. Nath, P.K. Saini, Dalton Trans. 40 (2011) 7077.
- [39] M. Nadvornik, J. Holecek, K. Handler, A. Lycka, J. Organomet. Chem. 275 (1984) 43.
- [40] J. Holecek, K. Handlir, M. Nadvornik, A. Lycka, J. Organomet. Chem. 258 (1983) 147.
- [41] T.S. Basu Baul, A. Paul, A. Linden, J. Organomet. Chem. 696 (2012) 4229.
- [42] T.P. Lochart, W.F. Manders, Inorg. Chem. 25 (1986) 892.
- [43] J. Bernstein, R.E. Davis, L. Shimoni, N.-L. Chang, Angew. Chem. Int. Ed. Engl. 34 (1995) 1555–1573.
- [44] Qing-Feng Wang, Chun-Lin Mab, Guo-Fang He, Zhen Li, Polyhedron 49 (2013) 175.
- [45] W. Maniukiewicz, E. Molins, C. Miravittles, J.-C. Wallet, E.M. Gaydou, J. Chem. Cryst. 26 (1996) 691.
- [46] R.S. Berry, J. Chem. Phys. 32 (3) (1960) 933.
- [47] A.W. Addison, T.N. Rao, J. Reedijk, J. van Rijn, G.C. Verschoor, J. Chem. Soc., Dalton Trans. (1984) 1349.
- [48] A.L. Spek, Acta Cryst. D 65 (2009) 148.
- [49] G. Matela, R. Aman, Cent. Eur. J. Chem. 10 (2012) 1.
- [50] T.S. Basu Baul, Appl. Organomet. Chem. 22 (2008) 195.
- [51] K.S. Singh, M. Roy, S. Roy, B. Ghosh, N.M. Devi, C.B. Singh, L.K. Mun, J. Coord. Chem. 70 (2017) 361.